

Supporting Information

An ICT based fluorescent reversible “ON-OFF-ON” switch for the selective and sequential detection of Hg²⁺ and I⁻ with application in imaging using human AGS gastric cancer cell

Saswati Gharami,^a Krishnendu Aich,^a Paramita Ghosh,^b Lakshman Patra,^a Nabendu Murmu^{*b} and Tapan K. Mondal^{*a}

^a Department of Chemistry, Jadavpur University, Kolkata-700032.

^b Department of Signal Transduction and Biogenesis Amines (STBA), Chittaranjan National Cancer Institute, Kolkata- 700026, India.

CONTENTS

Fig. S1. ¹H-NMR spectrum of compound 1

Fig. S2. ESI mass spectra of compound 1

Fig. S3. ¹H-NMR spectrum of BIPQ

Fig. S4. ¹³C-NMR spectra of BIPQ

Fig. S5. ESI mass spectra of BIPQ

Fig. S6. ¹H-NMR spectrum of BIPQ-Hg²⁺ complex

Fig. S7: HRMS of BIPQ-Hg²⁺ complex

Fig. S8: ¹H NMR titration of BIPQ after addition of 2 equivalent of HgCl₂ in DMSO-d₆

Fig. S9. Change in UV-Vis spectra of the probe (BIPQ) (10 μM) upon addition of 2 equivalent of various metal ions (10 μM)

Fig. S10. Change in UV-Vis spectra of BIPQ-Hg²⁺ (10 μM) upon addition of 2 equivalent of various anions (10 μM)

Fig. S11. Fluorescence change of compound 1, compound 1 + Hg²⁺ and compound 1 + Hg²⁺ + I⁻ (20 μM)

Fig. S12. Mole ratio plot of BIPQ for Hg²⁺ and I⁻

Fig. S13. Linear response curve of BIPQ depending on both Hg²⁺ and I⁻ concentration

Fig. S14. Job's plot of BIPQ for Hg²⁺

Fig. S15. Determination of association constant of BIPQ for Hg²⁺ from fluorescence titration data

Fig. S16. Lifetime decay profile of BIPQ, BIPQ-Hg²⁺ and BIPQ-Hg²⁺-I⁻

Fig. S17. Bar diagram plot of the relative emission intensity of BIPQ upon addition of various metal cations (10 μM) and Hg^{2+} (20 μM) in presence of other cations and of BIPQ- Hg^{2+} upon addition of various anions (10 μM) and I^- (20 μM) in presence of other anions

Fig. S18. Optimized structure of BIPQ calculated by DFT/B3LYP/6-31+G(d) method

Fig. S19. Optimized structure of BIPQ- Hg^{2+} calculated by DFT/B3LYP/6-31+G(d) method

Fig. S20. Contour plots of some selected molecular orbitals of BIPQ

Fig. S21. Contour plots of some selected molecular orbitals of BIPQ- Hg^{2+}

Fig. S22. Plot of IC_{50} dose of the probe (BIPQ) in AGS cells

Fig. S23. Determination of quantum yield for BIPQ and BIPQ- Hg^{2+}

Table S1. Energy and compositions of some selected molecular orbitals of BIPQ- Hg^{2+}

Table S2. Vertical electronic transitions calculated by TDDFT/B3LYP/CPCM method for SAPH and BIPQ- Hg^{2+} in methanol

Table S3. Crystallographic data and refinement parameters of BIPQ- Hg^{2+}

Table S4. Selected bond distances (\AA) and angles ($^\circ$) of BIPQ- Hg^{2+} complex

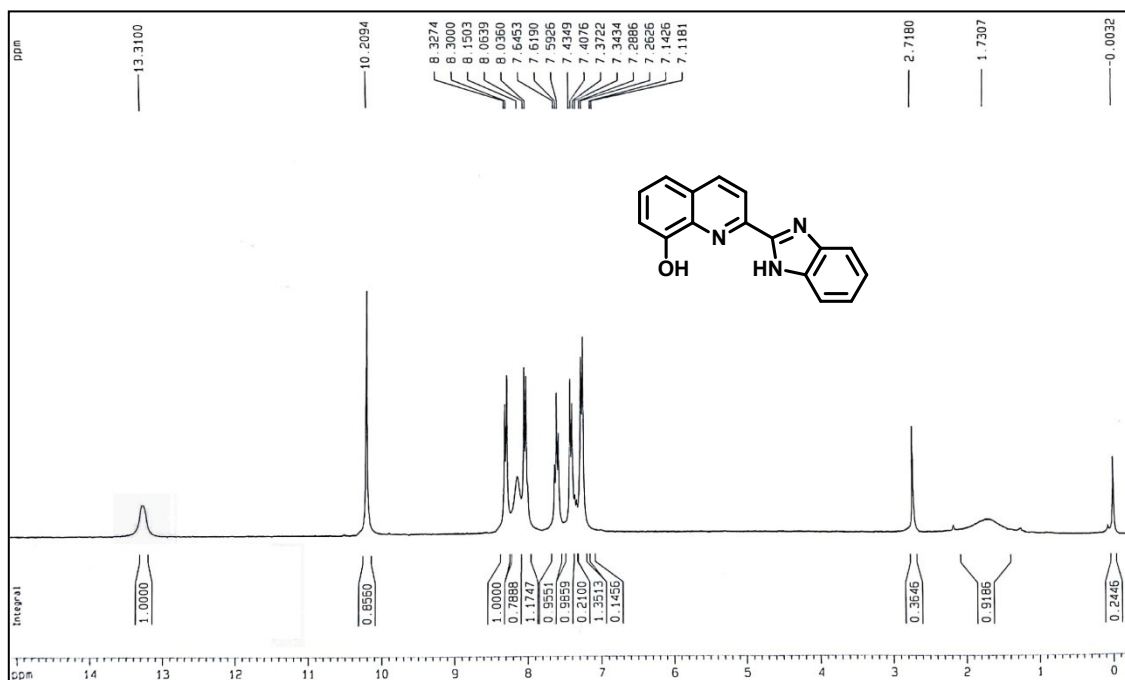


Figure S1: ^1H NMR (300 MHz) spectra of compound **1** in CDCl_3

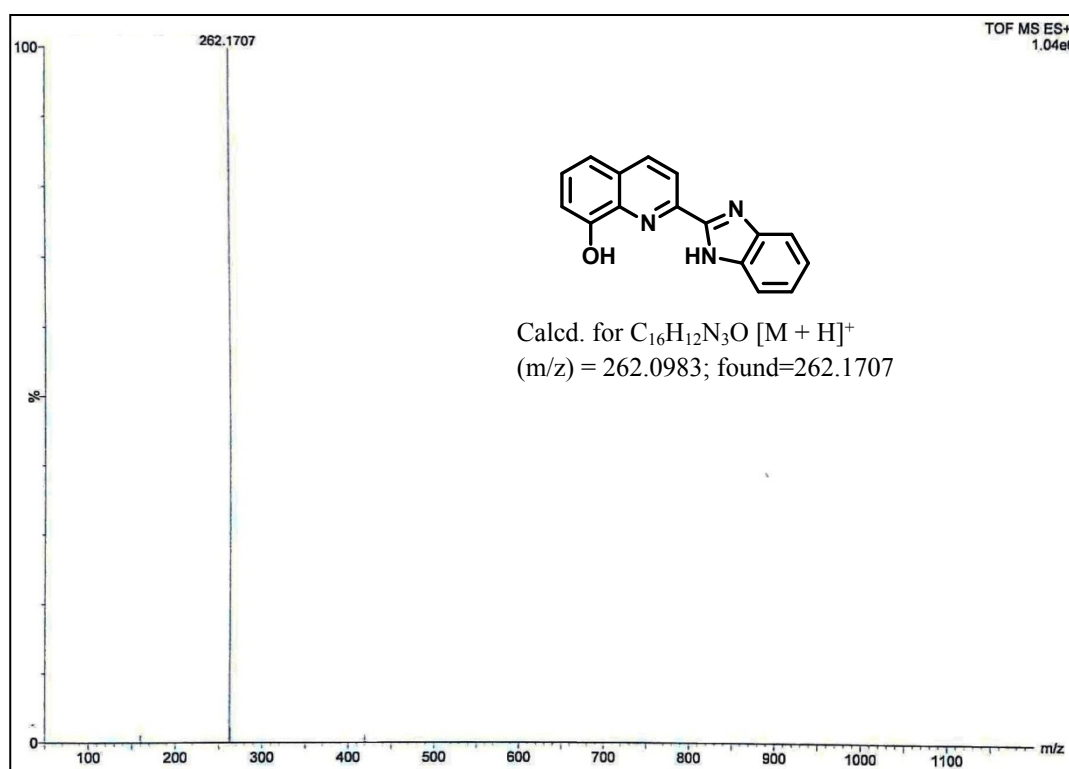


Figure S2: HRMS of Compound **1**

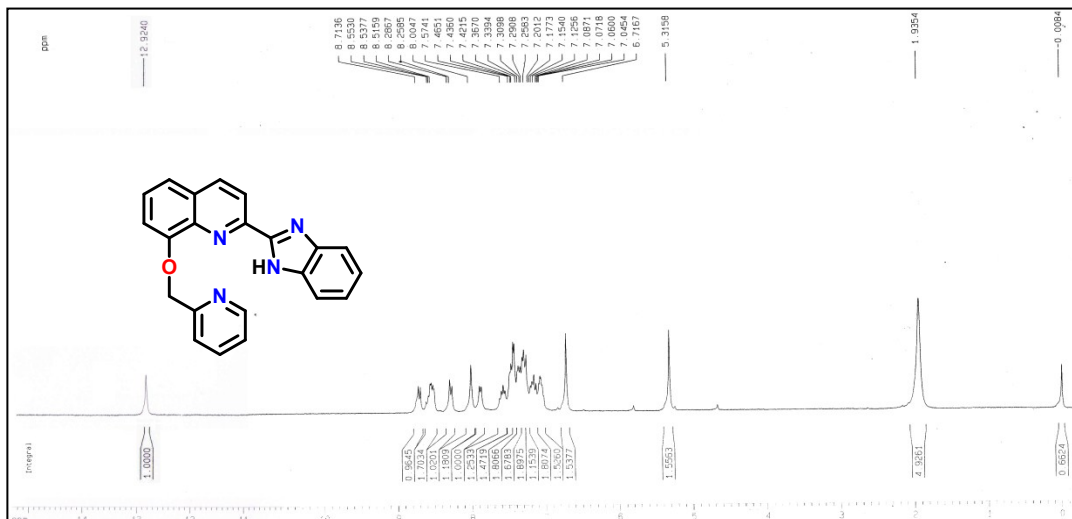


Figure S3: ^1H NMR (300 MHz) spectra of the probe (BIPQ) in CDCl_3

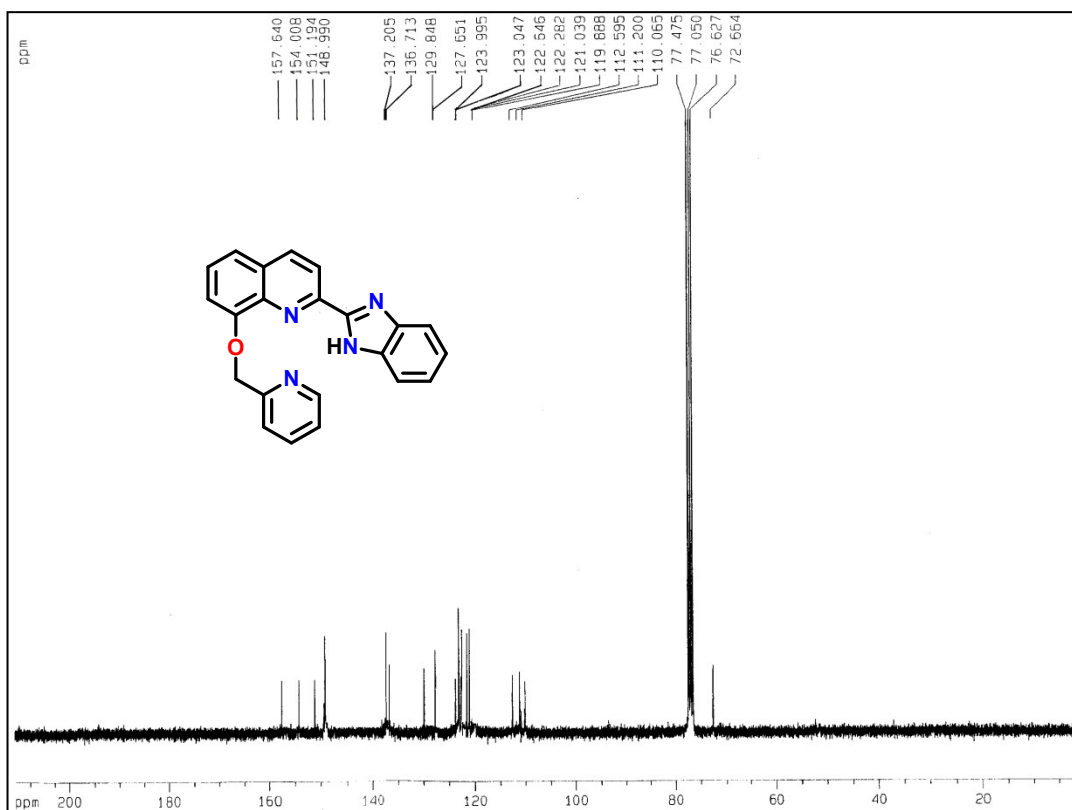


Figure S4: ^{13}C NMR (75 MHz) spectra of the probe (BIPQ) in CDCl_3

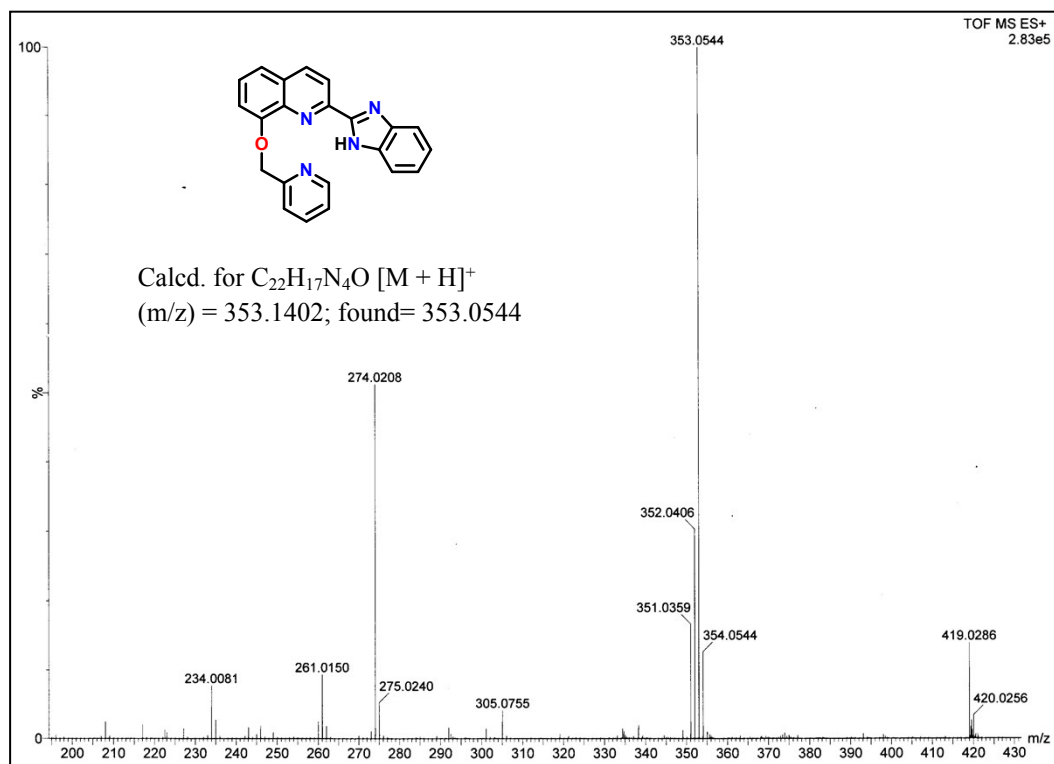


Figure S5: HRMS of the probe (BIPQ)

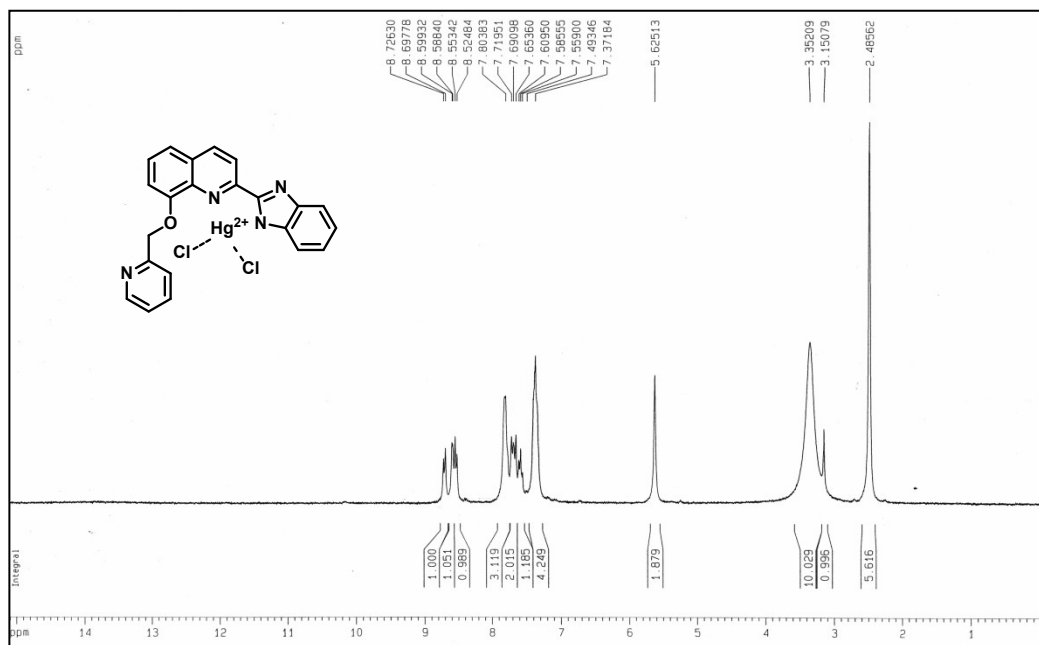


Figure S6: 1H -NMR spectrum of BIPQ-Hg²⁺ complex in DMSO-d₆

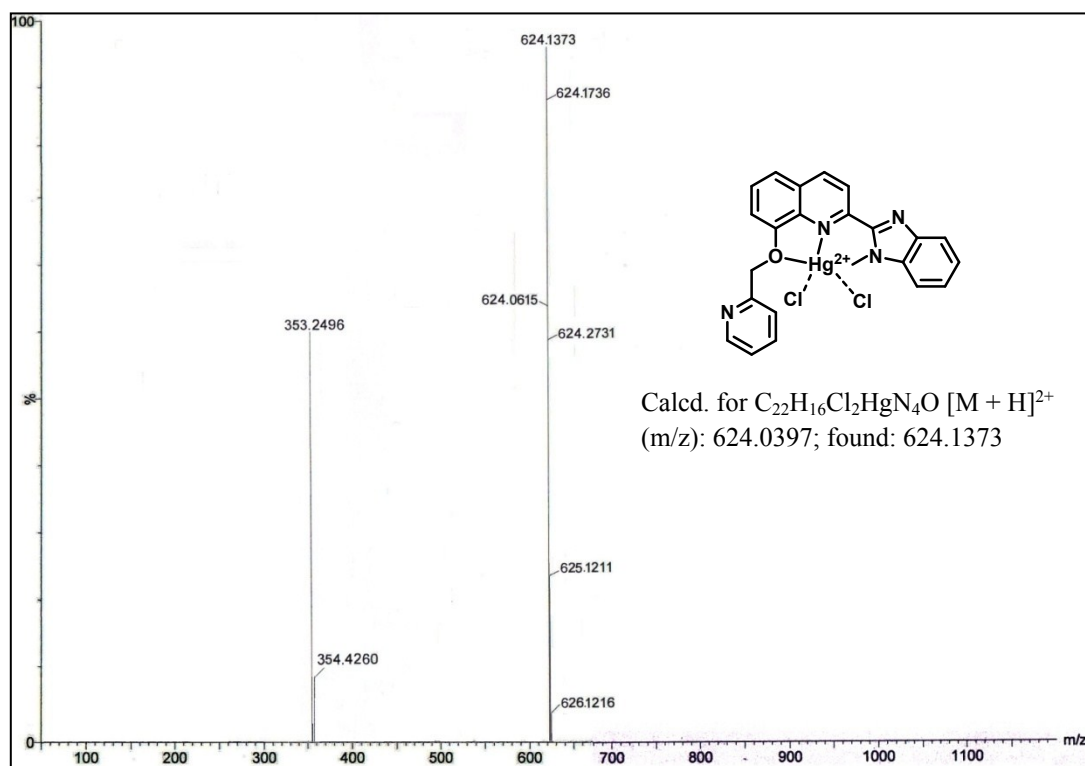


Figure S7: HRMS of BIPQ- Hg^{2+} complex

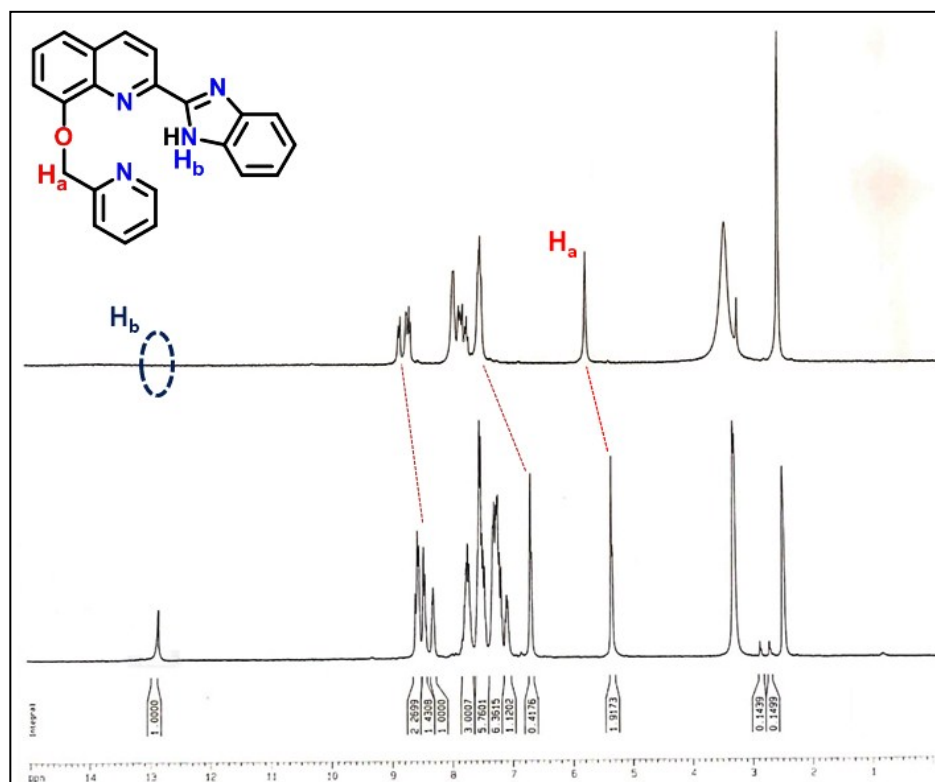


Figure S8: 1H NMR titration of BIPQ after addition of 2 equivalents of $HgCl_2$ in $DMSO-d_6$

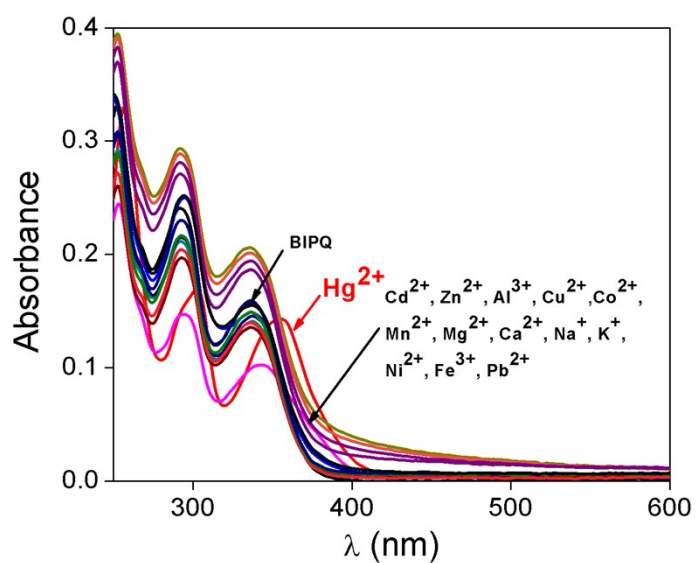


Figure S9: UV-vis change of BIPQ (10 μM) upon addition of different metal ions (2 equiv.)

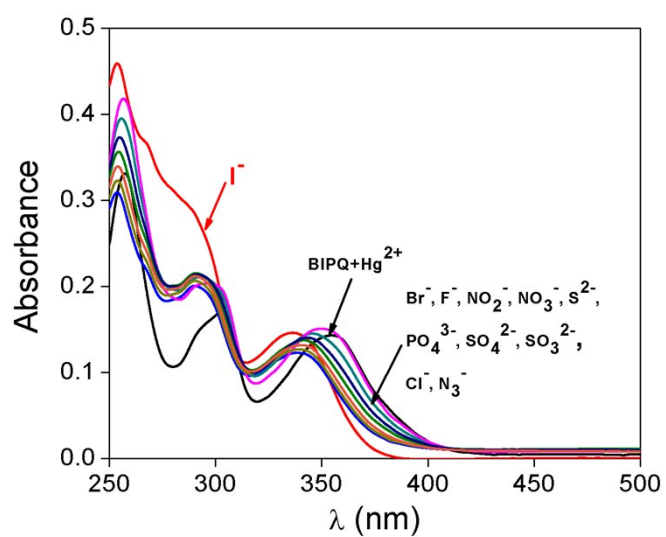


Figure S10: UV-vis change of BIPQ- Hg^{2+} (10 μM) upon addition of different anions (2 equiv.)

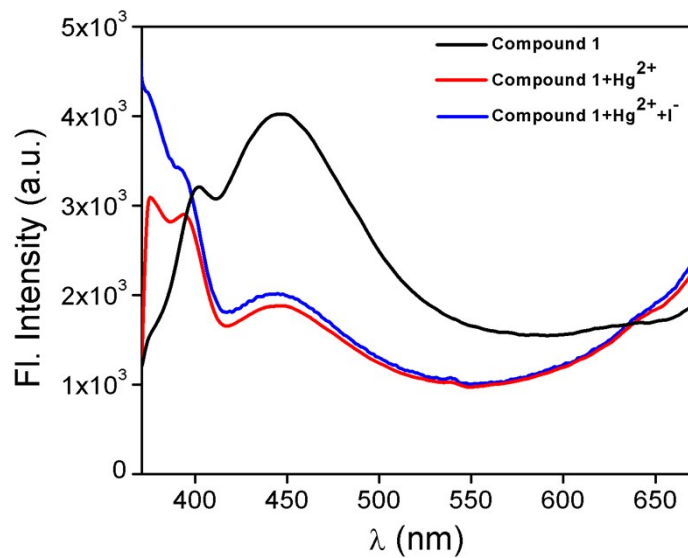


Figure S11: Fluorescence change of compound 1, compound 1 + Hg²⁺ and compound 1 + Hg²⁺ + I⁻ (20 μM)

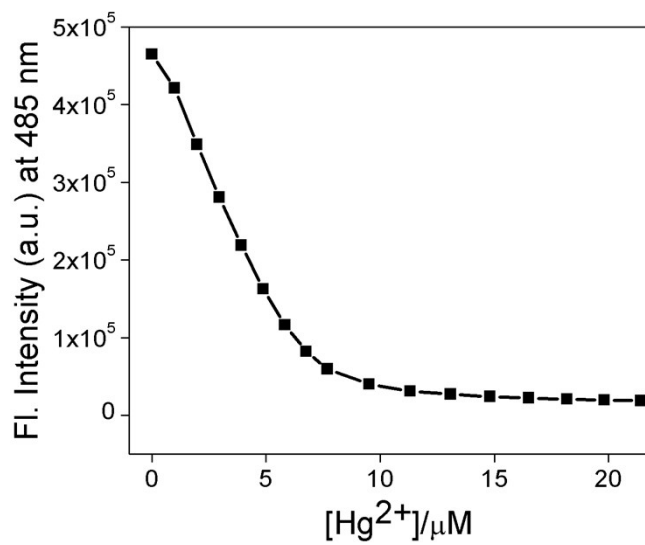


Figure S12a: Mole ratio plot of BIPQ for Hg²⁺

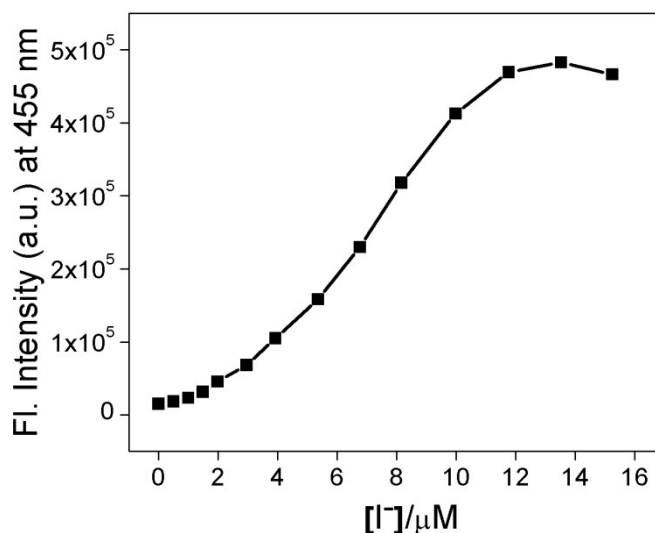


Figure S12b: Mole ratio plot of BIPQ-Hg²⁺ for I⁻

Determination of detection limit:

The limit of detection value was calculated based on the fluorescence titration of the developed probe. To determine the S/N ratio, the emission intensity of BIPQ without the ion, Hg²⁺ was measured by 10 times and the standard deviation of blank measurements was determined. Similarly, to determine the S/N ratio in case of I⁻, the emission intensity of BIPQ-Hg²⁺ without the presence of I⁻ was measured by 10 times and the value was calculated. So the detection limit of **BIPQ** and **BIPQ-Hg²⁺** for Hg²⁺ and I⁻ respectively were determined from the following equation:

$$DL = K \times Sb_1/S$$

Where K = 2 or 3 (we take 3 in this case); Sb₁ is the standard deviation of the blank solution; S is the slope of the calibration curve.

For Hg²⁺:

From the graph we get slope = 6.23×10^{10} and Sb₁ value is 64.94192

Thus using the formula we get the Detection Limit = 3.12×10^{-9} M i.e., BIPQ can detect Hg²⁺ in this minimum concentration by fluorescence technique.

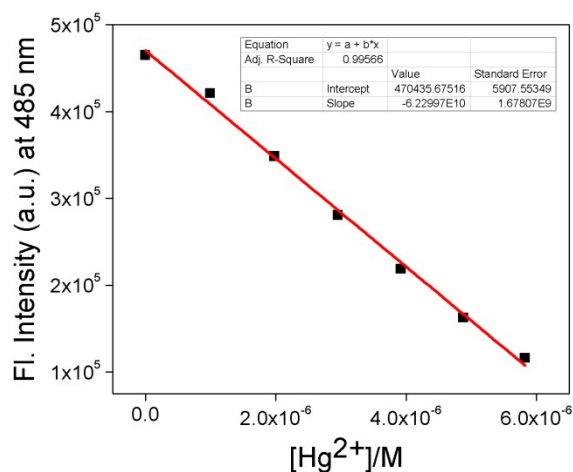


Figure S13a: Linear response curve of BIPQ at 485 nm depending on the Hg^{2+} concentration

For I⁻:

From the graph we get slope = 4.68×10^{10} and Sb_1 value is 854.88

Thus using the formula we get the Detection Limit = 5.48×10^{-8} M i.e., BIPQ- Hg^{2+} can detect I⁻ in this minimum concentration by fluorescence technique.

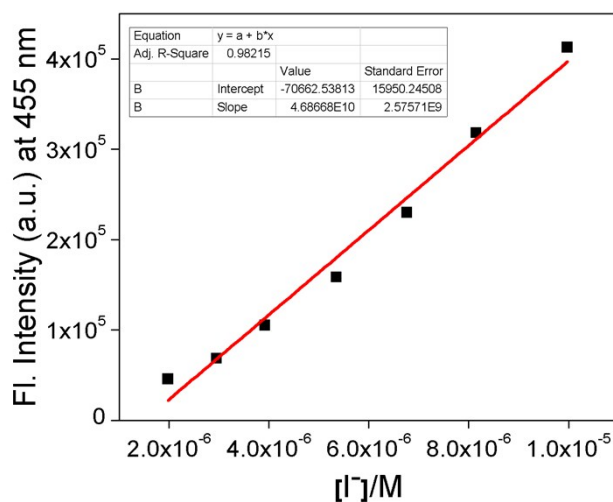


Figure S13b: Linear response curve of BIPQ- Hg^{2+} at 455 nm depending on the I⁻ concentration

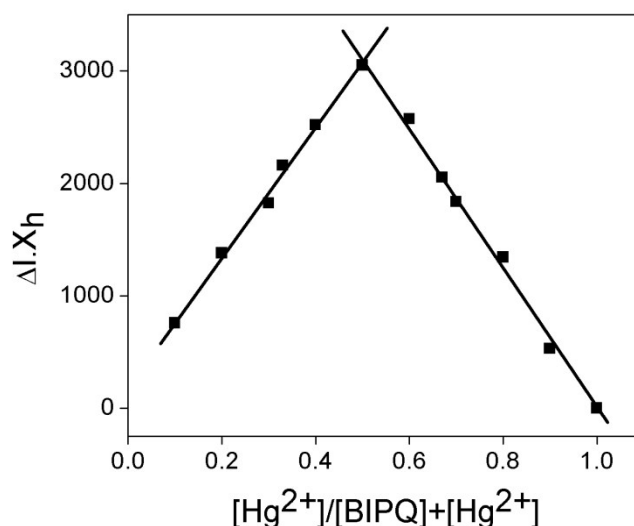


Figure S14: Job's plot of BIPQ for Hg²⁺

Determination of binding constant from Fluorescence titration data:

Binding constant was calculated according to the Benesi-Hildebrand equation. K_a was calculated following the equation stated below.

$$1/(F-F_0) = 1/\{K_a(F_{min}-F_0) [M^{n+}]^x\} + 1/[F_{min}-F_0]$$

Here F_0 , F and F_{min} indicate the emission in absence of, at intermediate and at infinite concentration of metal ion respectively.

Plot of $1/[F-F_0]$ vs $1/[Hg^{2+}]$ gives a straight line indicating 1:1 complexation between BIPQ and Hg²⁺ where K_a is found to be $1.4 \times 10^6 M^{-1}$ for BIPQ.

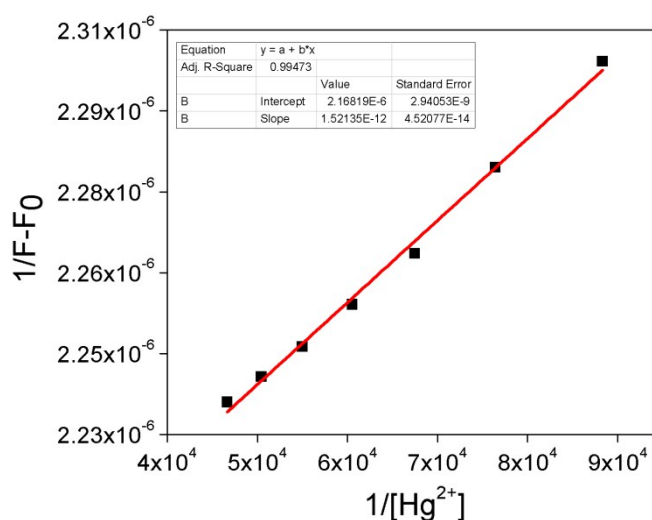


Figure S15: Determination of association constant of BIPQ at 485 nm depending on the Hg²⁺ concentration using Benesi-Hildebrand equation

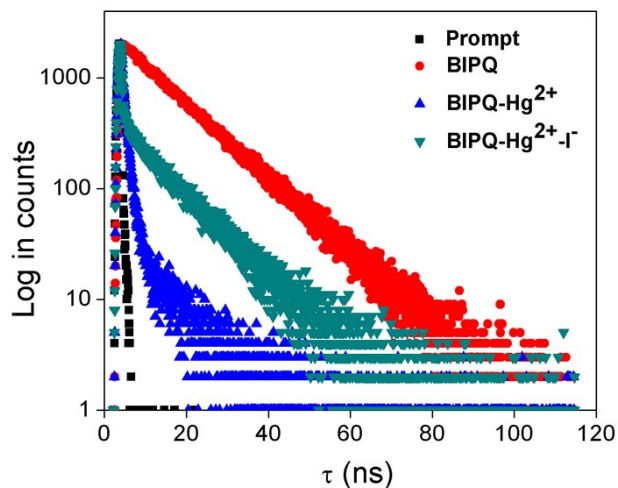


Figure S16: Lifetime decay profile of BIPQ, BIPQ-Hg²⁺ and BIPQ-Hg²⁺-I⁻

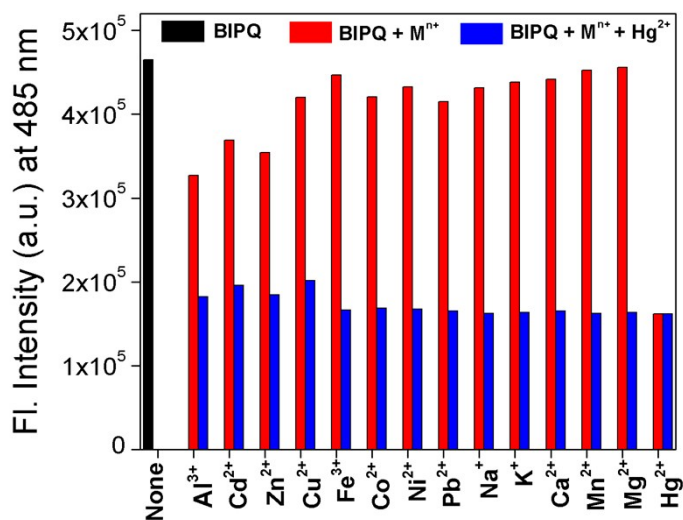


Figure S17a: Bar diagram representation of the relative emission intensity of BIPQ upon addition of various metals (10 μM) in MeOH:H₂O (1:4, v/v) (HEPES buffer, pH=7.4) (red bars) and Hg²⁺ (20 μM) in presence of other metal ions (blue bars)

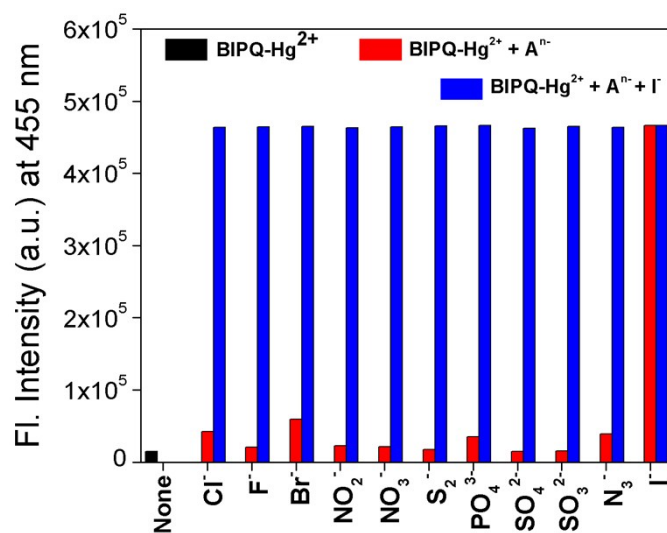


Figure S17b: Bar diagram representation of the relative emission intensity of BIPQ-Hg²⁺ upon addition of various anions (10 μM) in MeOH:H₂O (1:4, v/v) (HEPES buffer, pH=7.4) (red bars) and I⁻ (20 μM) in presence of other anions (blue bars)

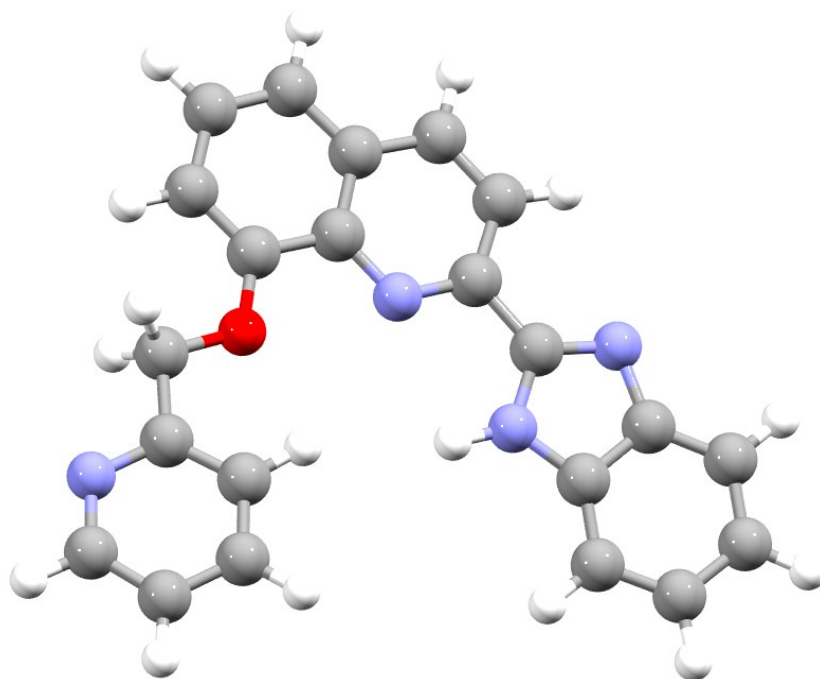


Figure S18. Optimized structure of BIPQ calculated by DFT/B3LYP/6-31+G(d) method

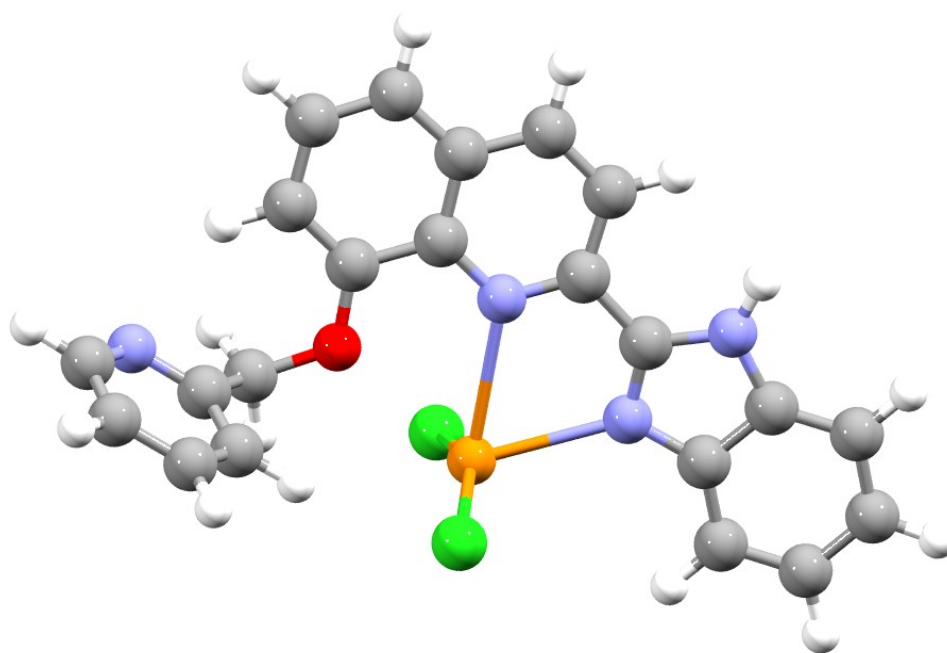


Figure S19. Optimized structure of BIPQ-Hg²⁺ calculated by DFT/B3LYP/6-31+G(d) method

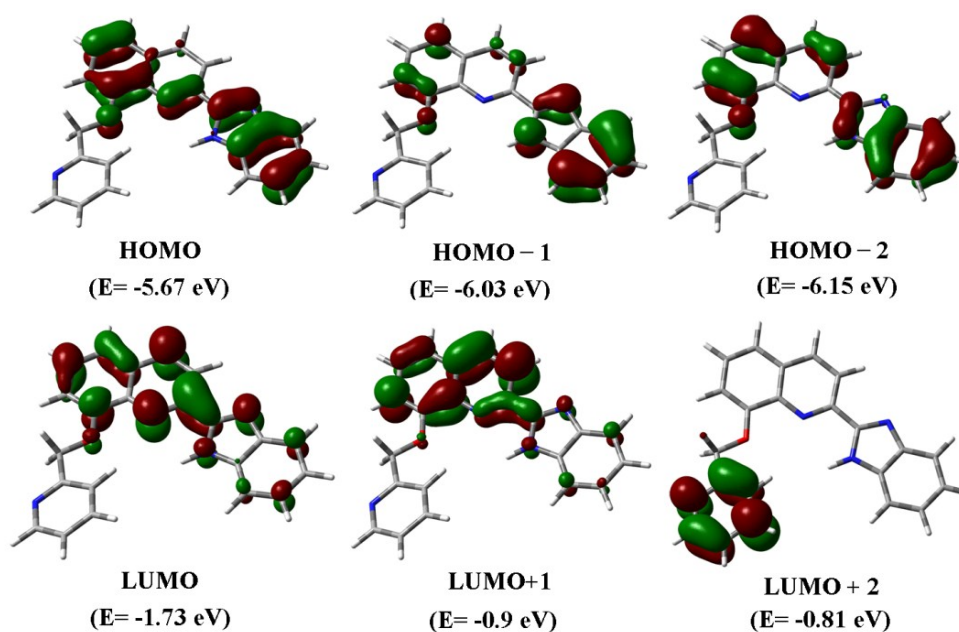


Figure S20. Contour plots of some selected molecular orbitals of BIPQ

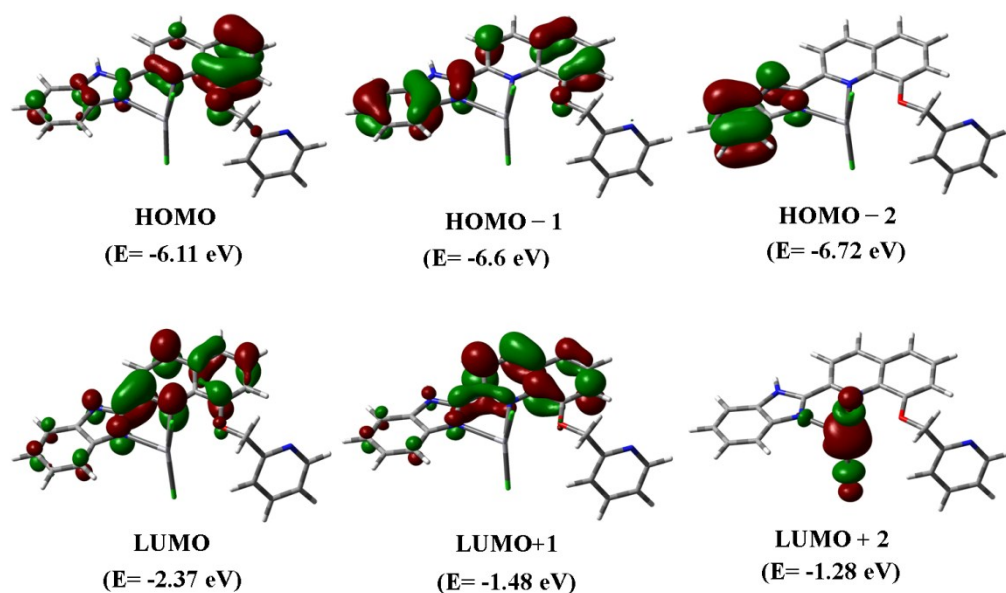


Figure S21. Contour plots of some selected molecular orbitals of BIPQ-Hg²⁺ complex

Table S1. Energy and compositions of some selected molecular orbitals of BIPQ-Hg²⁺

MO	Energy (eV)	% of composition		
		Hg	Cl	BIPQ
LUMO+5	-0.38	0	0	99
LUMO+4	-0.5	2	0	98
LUMO+3	-0.76	2	1	97
LUMO+2	-1.28	64	27	9
LUMO+1	-1.48	0	0	100
LUMO	-2.37	1	0	99
HOMO	-6.11	0	0	100
HOMO-1	-6.6	0	1	99
HOMO-2	-6.72	0	0	100
HOMO-3	-6.86	7	88	55
HOMO-4	-6.91	5	89	6
HOMO-5	-6.94	8	77	15
HOMO-6	-7.08	1	26	74

HOMO-7	-7.13	1	13	86
HOMO-8	-7.23	3	57	40
HOMO-9	-7.66	0	1	99
HOMO-10	-7.83	4	11	85

Table S2. Vertical electronic transitions calculated by TDDFT/B3LYP/CPCM method for BIPQ and BIPQ-Hg²⁺ in methanol

Compds.	Energy (eV)	Wavelength h (nm)	Osc. strength (f)	Transition	Character
BIPQ	3.4718	357.1	0.3442	(93%) HOMO→LUMO	$\pi(\text{L}) \rightarrow \pi^*(\text{L})$
	3.7708	328.8	0.3247	(73%) HOMO-1→LUMO	$\pi(\text{L}) \rightarrow \pi^*(\text{L})$
	3.9223	316.1	0.0261	(86%) HOMO-2→LUMO	$\pi(\text{L}) \rightarrow \pi^*(\text{L})$
	4.2372	292.6	0.5024	(77%) HOMO→LUMO+1	$\pi(\text{L}) \rightarrow \pi^*(\text{L})$
BIPQ-Hg ²⁺	3.2650	379.7	0.1887	(95%) HOMO→LUMO	$\pi(\text{L}) \rightarrow \pi^*(\text{L})$
	3.6932	335.7	0.4040	(88%) HOMO-1→LUMO	$\pi(\text{L}) \rightarrow \pi^*(\text{L})$
	3.8853	321.6	0.479	(98%) HOMO-1→LUMO	$\pi(\text{L}) \rightarrow \pi^*(\text{L})$
	3.9772	311.7	0.0024	(99%) HOMO→LUMO+1	$\pi(\text{L}) \rightarrow \pi^*(\text{L})$
	4.7054	263.5	0.0631	(56%) HOMO→LUMO+2	$\pi(\text{L}) \rightarrow \pi^*(\text{M})$

X-ray Data Collection and Crystal Structure Determination.

Details of crystal analysis, data collection and structure refinement data for BIPQ-Hg²⁺ complex is given in Table S3. Crystal mounting was done on glass fibers with epoxy cement. A red, niddle shaped single crystal of the BIPQ-Hg²⁺, with dimensions of 0.14 mm × 0.08 mm × 0.07 mm was selected and its X-ray analysis was done using Apex II CCDC diffractometer with fine-focus sealed tube graphite-monochromated Mo K α radiation ($\lambda = 0.71073$ Å) at room temperature. The data was processed with SAINT and a multi-scan absorption correction was performed using SADABS 2016/2 (Bruker, 2016).¹ wR₂(int) was 0.1103 before and 0.0557 after correction. The ratio of minimum to maximum transmission was 0.5694. The $\lambda/2$ correction factor was 0.0015. The structure was solved by direct method using the program SHELXTL² and was refined by full-matrix least squares technique on F² using anisotropic displacement parameters for all non-hydrogen atoms. Hydrogen atoms were included in the refinement process as per the riding model. Crystallographic data have been deposited at the Cambridge Crystallographic Data Centre with CCDC 1914359 for BIPQ-Hg²⁺. Copies of the data can be obtained free of charge on application to the CCDC, 12 Union Road, Cambridge CB2 IEZ, UK. Fax: +44-(0)1223-336033 or e-mail: deposit@ccdc.cam.ac.uk.

Table S3: Crystallographic data and refinement parameters of BIPQ-Hg²⁺

Formula	C ₂₂ H ₁₆ Cl ₂ HgN ₄ O
Formula Weight	623.88
Crystal System	<i>Triclinic</i>
Space group	<i>P -1</i>
a, b, c [Å]	7.5222 (6), 6.2463 (7), 16.0762 (12)
α	75.104 (2)
β	89.593 (2)
γ	79.724 (2)
V [Å ³]	1062.35 (14)
Z	2
D(calc) [g/cm ³]	1.950
μ (Mo K α) [mm ⁻¹]	7.517
F(000)	596
Absorption Correction	<i>multi-scan</i>
Temperature (K)	273
Radiation [Å]	0.71073
θ (Min-Max) [°]	2.25- 22.00
Dataset (h; k; l)	-9 and 9; -11 and 11; -20 and 20
Total, Unique Data, R(int)	36664/4673/0.0363
Observed data [I > 2 σ (I)]	4399
Nref, Npar	4673/275
R, wR ₂	0.0179, 0.0440
Δq (max) and Δq (min) [e/Å ³]	0.503 and -0.829
Goodness of fit(S)	1.012

Table S4: Selected bond distances (Å) and angles (°) of BIPQ-Hg²⁺ complex

Bonds (Å)	BIPQ-Hg ²⁺
Hg1-N1	2.293(2)
Hg1-N3	2.407(2)
Hg1-O1	2.7161(19)
Hg1-Cl1	2.4678(7)
Hg1-Cl2	2.3533(8)
Angles (°)	
N1-Hg1-N3	71.51(7)
N1-Hg1-O1	133.76(6)
N1-Hg1-Cl1	108.38(6)
N1-Hg1-Cl2	118.72(6)
N3-Hg1-O1	62.57(6)
N3-Hg1-Cl1	101.51(5)
N3-Hg1-Cl2	134.03(5)
O1-Hg1-Cl1	86.53(5)
O1-Hg1-Cl2	91.15(5)
Cl1-Hg1-Cl2	114.54(3)
trigonal index τ	0.005

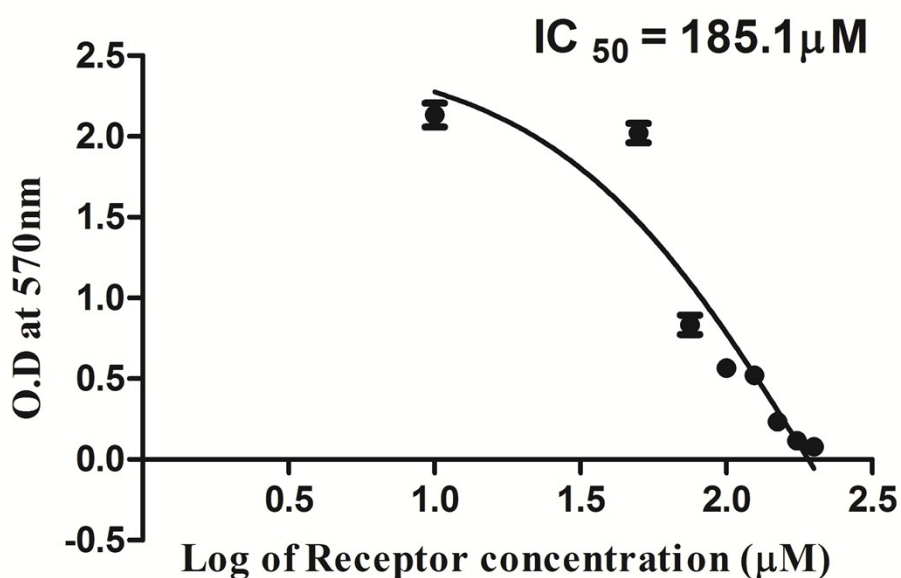
Determination of fluorescence Quantum Yield (ϕ) of BIPQ and BIPQ-Hg²⁺.

The fluorescence quantum yield was determined using quinine sulfate as the reference dye. For the deduction of the quantum yields of BIPQ and its complex with Hg²⁺, the absorbance of both the compounds were recorded in methanol solution. After that the emission spectra was recorded using the maximal excitation wavelengths and the integrated areas of the spectra were calculated further. The quantum yields were then measured by comparing with that of the reference dye, i.e., the quinine sulfate here ($\phi_s = 0.54$ in 0.5 M sulfuric acid) using the following equation:

$$\Phi_x = \Phi_s \times \left(\frac{I_x}{I_s}\right) \times \left(\frac{A_s}{A_x}\right) \times \left(\frac{n_x}{n_s}\right)^2$$

Where, x & s designate the unknown and standard solution respectively, ϕ is the quantum yield, I is the integrated area under the fluorescence spectra, A is the absorbance and n is the refractive index of the solvent.

So the quantum yields of BIPQ, BIPQ-Hg²⁺ and BIPQ-Hg²⁺-I⁻ are calculated using the above equation and the values are 0.56, 0.15 and 0.54 respectively.



S22: IC₅₀ dose of the probe (BIPQ) in AGS cells; calculated to be 185.1 µM

References:

1. Bruker (2018). Apex3 v2017.3-0, Saint V8.38A, SAINT V8.38A, Bruker AXS Inc.: Madison (WI), USA, 2018.
2. Sheldrick G. M. A short history of SHELX. *Acta Cryst.* **2008**, A64, 112-122.